Journal of Physics:
Condensed Matter

PAPER • **OPEN ACCESS**

Magnetic anomaly and field-dependent properties of Gd^{3+} in $GdTe_{1.8}$

To cite this article: Jörg Sichelschmidt *et al* 2026 *J. Phys.: Condens. Matter* **38** 305801

Journal of Physics: Condensed Matter

PAPER

OPEN ACCESS

RECEIVED
11 February 2026

REVISED
3 July 2026

ACCEPTED FOR PUBLICATION
14 July 2026

PUBLISHED
27 July 2026

Magnetic anomaly and field-dependent properties of Gd^{3+} in $GdTe_{1.8}$

Jörg Sichelschmidt[1,*], Ellen Häußler[2], Jorge Galeano-Cabral[3,4], Kaya Wei[3], Thomas Doert[2] and George S Nolas[5]

[1] Max Planck Institute for Chemical Physics of Solids, Dresden, Germany
[2] Faculty of Chemistry and Food Chemistry, TUD Dresden University of Technology, Dresden, Germany
[3] National High Magnetic Field Laboratory, Florida State University, Tallahassee, FL 32310, United States of America
[4] Department of Materials Science and Engineering, North Carolina State University, Raleigh, NC 27606, United States of America
[5] Department of Physics, University of South Florida, Tampa, FL 33624, United States of America
[*] Author to whom any correspondence should be addressed.

E-mail: Sichelschmidt@cpfs.mpg.de and gnolas@usf.edu

Keywords: binary rare-earth metal chalcogenides, magnetocaloric materials, thermoelectric materials, electron spin resonance, magnetic order

Supplementary material for this article is available online

Abstract

The magnetic properties of Gd^{3+} in polycrystalline $GdTe_{1.8}$ were investigated by magnetization, heat capacity, magnetoresistance, and electron spin resonance (ESR) which all reveal clear indications of a magnetic phase transition at ≈11 K in their temperature dependencies. The transition displays characters of competing ferromagnetic and antiferromagnetic interactions which is particularly supported by distinct anomalies in the ESR linewidth and intensity, providing a local picture of magnetism at the transition. A pronounced negative magnetoresistance documents a strong coupling between magnetic order and charge transport in the puckered GdTe double layers that form the $GdTe_{1.8}$ crystal structure.

1. Introduction

Binary metal chalcogenides are a class of inorganic materials that continue to be of interest due to their diverse and exceptional physical and chemical properties, that lend themselves to a variety of applications [1, 2]. For example, GeTe has been investigated for potential phase-change memory applications [3] while the high mobility van der Waals layered material $GdTe_3$ is of potential interest for spintronics applications [1]. The charge transport in chalcogenides of *d*- and *f*-metals is often impeded by a strong coupling to magnetic degrees of freedom as indicated by a sizeable magnetoresistance. In general, the layered structure may favor competing ferromagnetic (FM) and antiferromagnetic (AFM) interactions determining complex magnetic properties which can sensitively depend on composition [4, 5], structural vacancies [6, 7], or multiple inequivalent sites of the magnetic ion [8–10].

In this work we investigate the interplay between FM and AFM magnetic order of the semiconductor $GdTe_{1.8}$. We suggest that this interplay originates from the complex structural properties of $GdTe_{1.8}$ which belongs to the binary rare-earth metal polychalcogenide family of compounds with the general composition $REX_{2-\delta}$ (RE = Y, La -Nd, Sm, Gd-Lu; X = S, Se, Te). These compounds show a large structural variety in a comparatively small compositional range ($0 \leqslant \delta \leqslant 0.2$) originating from chalcogen defects [11–13]. The structures are all superstructures of the ZrSSi-type structure (space group $P4/nmm$) and consist of an alternating stacking of puckered REX slabs and planar X layers in which the chalcogen vacancies are solely found [12]. $GdTe_{1.8}$ crystallizes in a $\sqrt{5}\cdot\sqrt{5}\cdot 2$-fold superstructure of the aristotype in space group $P4/n$, its planar Te layers consisting of dumbbell-shaped Te_2^{2-} anions and linear Te_3^{4-} anions [14], see figure 1. In a previous contribution, $GdTe_{1.8}$ has been described as paramagnetic down to 2 K, although a kink in the susceptibility curve already indicated a magnetic transition near

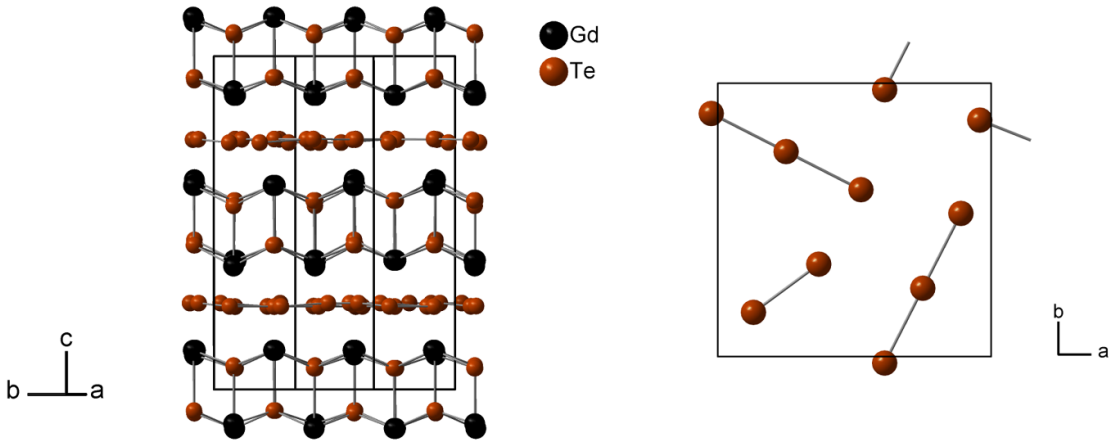

Figure 1. Crystal structure of $GdTe_{1.8}$ emphasizing the stacking of puckered GdTe slabs and planar Te layers along the [001] direction (left) and view on the Te layer featuring its Te_2^{2-} and Te_3^{4-} anions (right).

11 K [14]. We therefore decided to re-investigate $GdTe_{1.8}$ to elucidate the nature of the magnetic transition by measurements of the heat capacity, magnetoresistance and electron spin resonance (ESR), the latter being a direct local probe of the Gd^{3+} ($S = 7/2$) magnetism. We will also qualitatively compare the ordering temperatures of different gadolinium tellurides which comprise the same structural features.

2. Experimental

All steps for the synthesis and sample handling of $GdTe_{1.8}$ were carried out under inert conditions. In a standard synthesis, 3 g of a stoichiometric mixture of Gd_2Te_3, tellurium (Alfa Aesar, 99.999%) and a small amount of iodine ($\approx$0.02 equivalents to $GdTe_{1.8}$) were placed in a silica ampoule which was then sealed under dynamic vacuum ($p \leqslant 1 \cdot 10^{-3}$ mbar). The iodine serves to enhance mass transport via a short-range chemical vapor reaction and to ensure a complete reaction. The reaction mixture was heated to 1073 K and held at this temperature for 5 days. The precursor Gd_2Te_3 was prepared by reacting elemental Gadolinium (99.5%, MaTecK) and tellurium (Merck, >99.9%, reduced in a hydrogen stream at 670 K prior to use) in a glassy carbon crucible inside a fused silica ampoule. The fine ground powder was heated to 1073 K and held at this temperature for four days. The purities of precursor and target compound were checked by powder x-ray diffraction on a Panalytical XPert Pro diffractometer in Bragg–Brentano geometry with Cu$K\alpha_1$ radiation (see plot of the Rietveld refinement of $GdTe_{1.8}$ in the Supplementary materials). The composition of selected particles was checked by energy-dispersive x-ray spectroscopy with a Silicon Drift Detector X-Max^N (Oxford Instruments) implemented in a scanning electron microscope SU8020 (Hitachi).

The magnetization was measured on a powder sample in a vibrating sample magnetometer (vsm) as part of a cryogen-free measuring system (mini-CFMS, Cryogenic Ltd, London) between 2 and 300 K. Temperature-dependent isobaric heat capacity, C_p, data were measured from 2 K to 100 K using a Quantum Design Physical Property Measurement System (PPMS) under constant magnetic fields of 0, 3, 6, and 9 T. The specimen was fixed to the sample holder using Apiezon N-grease, and the measured contribution of the addenda was subtracted from the total heat capacity. The measurement uncertainties, estimated from the relative standard error, were below 1% at low temperatures (T<15K), and between 1 and 2.5% for T>15K up to 100 K. Electrical resistivity, ρ, was measured using the four-point probe method, where platinum wires with diameter 0.025 mm were attached with silver paint to the sample with approximate dimensions of $1.5 \times 0.6 \times 0.1$ mm^3. The measurements were performed from 2 K to 400 K again using a PPMS under constant magnetic fields of 0, 3, 6, and 9 T. The uncertainties in ρ as estimated from the relative standard deviation were below $\sim$5% for T<250 K or $\sim$8% for T>250 K, respectively.

ESR measurements at X-band frequency ($\nu = 9.4$ GHz) were performed with a standard continuous-wave spectrometer on a polycrystalline sample of $GdTe_{1.8}$ (3.15 mg) in a temperature range between 4 and 300 K. The ESR setup detects the power, P, absorbed by the sample from a magnetic microwave field as a function of an external, transverse magnetic field B. A lock-in technique was used to improve the signal-to-noise ratio which yields the derivative of the resonance signal dP/dB as the measured

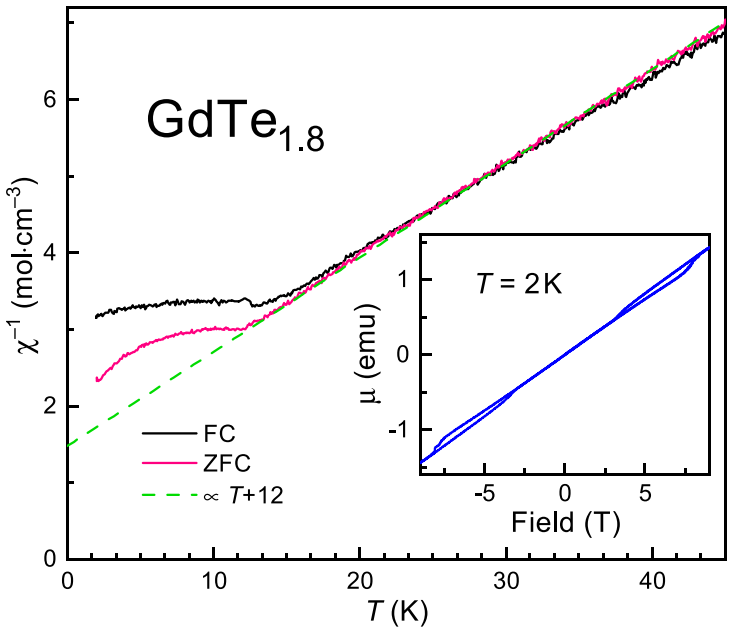

Figure 2. Temperature dependence of the inverse magnetic susceptibility $\chi^{-1}(T)$ per Gd atom for a field of 100 mT under field-cooled (FC) and zero-field-cooled (ZFC) conditions. Dashed line indicates Curie–Weiss law with $\theta = -12$ K. Inset: Hysteretic field dependence at $T = 2$ K of the magnetization as expressed by the effective magnetic moment μ.

quantity. All spectra were fitted by a symmetrical Lorentzian shape including the influence of the counter-rotating component of the linearly polarized microwave field [5]. From these fits we obtained the parameters linewidth (ΔB being a measure of the spin dynamics), resonance field ($B_{\rm res}$, as given by the resonance condition $h\nu = g\mu_B \cdot B_{\rm res}$ and being determined by the g-value and internal fields), and the amplitude (Amp). The ESR intensity $I_{\rm ESR}$ is deduced from the integrated ESR spectra and is a measure of the local spin susceptibility.

3. Results and discussion

As published previously the magnetic susceptibility $\chi(T)$ of $GdTe_{1.8}$ shows paramagnetic behavior down to $T \approx 20$ K with an effective magnetic moment of $7.48\mu_B$ [14]. Although a small kink in $\chi(T)$ near 11 K was already visible it was not discussed. The presence of this kink motivated further investigations on this compounds, the result of which is presented in the following.

Figure 2 displays in the main frame the low-temperature section of the previous $\chi(T)$-data [14] together with a Curie–Weiss temperature dependence ($\propto (T-\Theta)^{-1}$, dashed line). A negative Weiss temperature $\Theta = -12$ K well describes the data in the paramagnetic regime. This indicates the presence of antiferromagnetic correlations, consistent to the now clearly visible kink in $\chi(T)$ near 11 K being a typical signature expected for AFM order below $T_N = 11$ K. However, below $\approx$20 K the kink structure displays varying characteristics depending on whether FC or ZFC conditions were applied. We suspect that these FC/ZFC anomalies are due to ferromagnetic couplings which could also explain the weak, somewhat peculiarly shaped hysteretic field dependence of the magnetization at 2 K, see inset of figure 2. Similar weak hysteresis were reported for $GdTe_3$ [15] and for Gd_2Se_3; for the latter compound, this was attributed to meta-magnetic spin-flop transitions [16]. $GdTe_{1.875\pm\delta}$, however, with a composition being only slightly different from that of $GdTe_{1.8}$ but with a different ordering pattern in its planar Te layers, shows no FC/ZFC difference below the ordering temperature of $T_N = 11$ K [13]. Whether these differences between FC and ZFC are due to subtle differences in composition or in the precise arrangement of the atoms remains unclear at this time.

Figure 3(a) shows the temperature dependent C_p data between 1.8 K and 100 K under different applied magnetic fields. In zero field, C_p decreases with decreasing temperature down to approximately 15 K below which a pronounced maximum develops near 10 K and a minute kink around 7 K (see also figure 3(b). We note that multiple close-by magnetic phase transitions seem to be inherent to these materials as evidenced by the similarity in the C_p features of structurally related $GdTe_2$ [17] and $GdTe_3$ [18, 19]. Upon applying a magnetic field, the overall shape of $C_p(T)$ remains similar; however, the

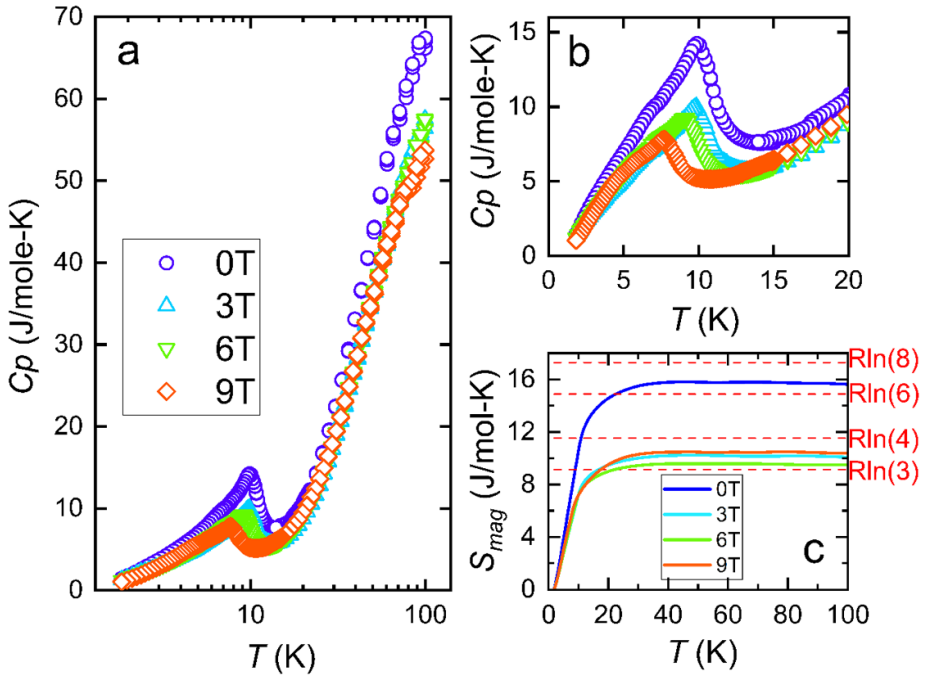

Figure 3. (a) Temperature-dependent specific heat C_p under the constant magnetic fields indicated, (b) expanded view of the low temperature region, and (c) the change in magnetic entropy as a function of temperature, as described in the text.

magnitude of C_p near 100 K decreases with increasing magnetic field indicating a broad suppression of magnetic contributions in the paramagnetic regime. As shown in figure 3(b), the peak and the minute kink near 10 K and 7 K, respectively, are progressively suppressed with increasing field strength. This suppression is a characteristic feature for a transition into AFM ordering and is reflecting a reduction in the available magnetic entropy of the system.

To further investigate this field-induced effect, the magnetic entropy, S_{mag}, shown in figure 3(c), was calculated using

$$S_{mag} = \int_0^T \frac{C_{mag}}{T} dT \tag{1}$$

where C_{mag} represents the magnetic contributions to the heat capacity obtained by subtracting the experimental data to a theoretical electronic and lattice contribution expressed as

$$C_p(T) = \gamma T + C_D \ (T/\theta_D)^3 \int_0^{\theta_D/T} \frac{x^4 e^x}{(e^x - 1)^2} dx \tag{2}$$

Here γT is the electronic contribution to C_p, $x = \frac{\hbar\omega}{\kappa_B T}$, ω is the Debye frequency, θ_D is the Debye temperature, and C_D is a constant that contains the numbers of oscillators and degrees of freedom. At zero field S_{mag} saturates near 30 K to a value that is below R ln(8), which is the theoretical value expected for the full Hund's rule multiplet of trivalent Gd ($J = 7/2$), where $-\Delta S_{max} = R\ln(2J+1) = R\ln(8)$. The deviation from the theoretical limit can be attributed to residual crystal-field effects [20] and magnetic interactions, which constrain the full release of entropy [21]. The magnitude of the deviation is comparable to that of other Gd compounds [22]. With increasing magnetic fields, the total recovered entropy decreases, and the saturation shifts downward reflecting the progressive lifting of the ground-state degeneracy and the corresponding reduction in accessible magnetic states. This behavior further supports the suppression of the magnetic degrees of freedom inferred from the field-dependent C_p data. Gd and Gd alloys are known to display strong magnetocaloric effects [23, 24], and these results suggest that $GdTe_{1.8}$ may be of interest for potential low temperature magnetocaloric applications as well.

In order to further characterize the field-dependent properties of $GdTe_{1.8}$, the magnetoresistance was also investigated. Figure 4 shows the temperature dependence of the resistivity $\rho(T)$ at magnetic fields of 0, 3, 6, and 9 T. The resistivity ρ increases sharply with decreasing temperature below approximately 20 K, particularly in zero field. However, this increase in ρ is strongly suppressed by applied magnetic

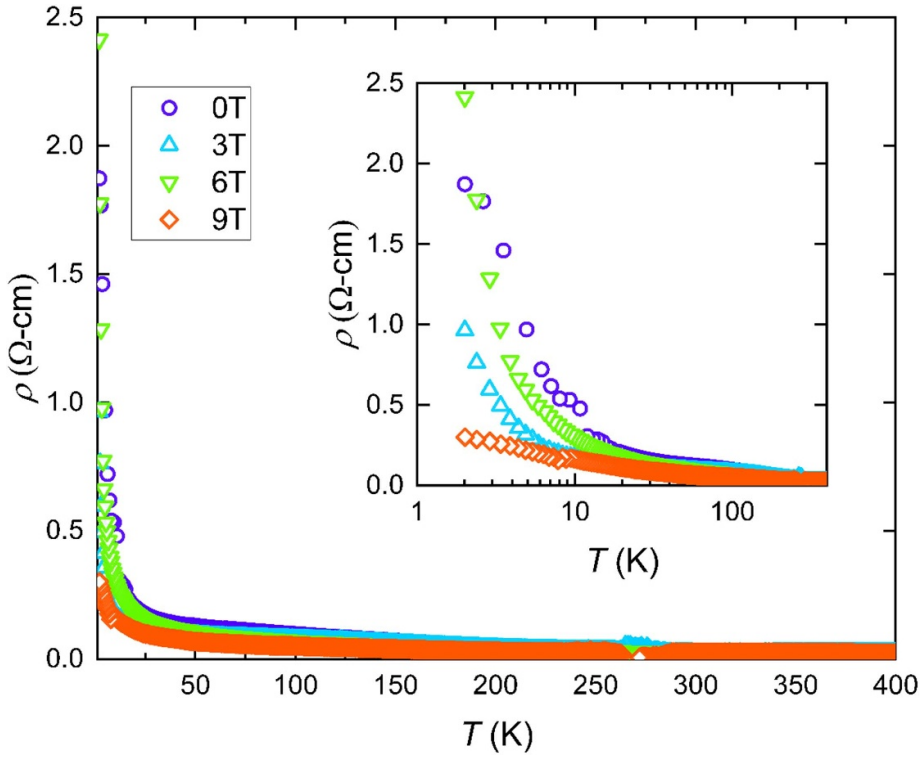

Figure 4. Temperature-dependent electrical resistivity ρ in the magnetic fields indicated. The inset shows the data in a log plot.

fields leading to a pronounced negative magnetoresistance. Such behavior can be attributed to spin-disorder scattering from the localized Gd^{3+} moments; in zero field random spin orientations enhance the electron scattering whereas an applied magnetic field aligns the moments and reduces spin fluctuations and thus lowers the resistivity [25]. Both field-induced suppressions, as observed by the peak in C_p and a decrease in ρ at low temperatures, provide consistent evidence for strong coupling between the localized 4*f* magnetic moments and the conduction electrons.

The properties of the transition at 11 K described so far predominantly favor magnetic ordering of AFM type. Nevertheless, some properties such as the weak hysteresis in the field-dependent magnetization (see inset of figure 2) are rather consistent with the presence of FM order. In this respect it is worth to point out the resemblance of the above presented field-dependent C_p data with the field-induced shifts in the C_p data of $GdTe_3$ single crystals [19]. There, the better resolved C_p data allowed to identify four magnetic phases: paramagnetic, partial AFM order, FM in AFM order, and perfect AFM order. Therefore, it is interesting to check for a corresponding "FM in AFM" phase also in our $GdTe_{1.8}$ sample. To this end ESR is a suitable method because it allows a direct and local access to the Gd^{3+} ($S = 7/2$) magnetism. As shown in figure 5(a) well defined Gd ESR signals could be observed. In this figure the solid lines indicate a fit by single symmetrical Lorentzian line shapes which well determine ΔB, B_{res} and *Amp*. The right panel of figure 5 shows the temperature dependencies of these parameters, with the intensity I_{ESR} being estimated by $Amp \cdot \Delta B^2$. A continuous broadening of the line results as the temperature decreases until $T \approx 9$ K, where a distinct anomaly appears. As described above, this anomaly is also clearly visible in our temperature-dependent C_p data. Moreover, the intensity shows a pronounced drop (see the insets in figures 5(b) and (d)). These conspicuous anomalies are not seen in the resonance field, figure 5(c), which shows a continuous deviation from the high temperature value corresponding to $g = 2.020(1)$.

Above $T \approx 10$ K the ESR intensity can be well described by a Curie–Weiss law $\propto (T - \theta)^{-1}$ (dashed line in figure 5(d) with $\theta = -12$ K, in agreement with magnetization data, see figure 2 and reference [14], implying overall antiferromagnetic interactions between the Gd ions. Below $T \approx 8$ K, within experimental error, the Curie–Weiss behavior may continue with the same value of θ but with a strongly altered slope. This points to a considerable ($\approx$17%) reduction of the number of paramagnetic, overall antiferromagnetically correlated, Gd moments. Furthermore, as shown by the dashed line in figure 5(c), the temperature dependence of the resonance field shows a Curie–Weiss dependence $\propto (T - 8)^{-1}$ K above $T \approx 10$ K that follows the form of the magnetization, a behavior which is found

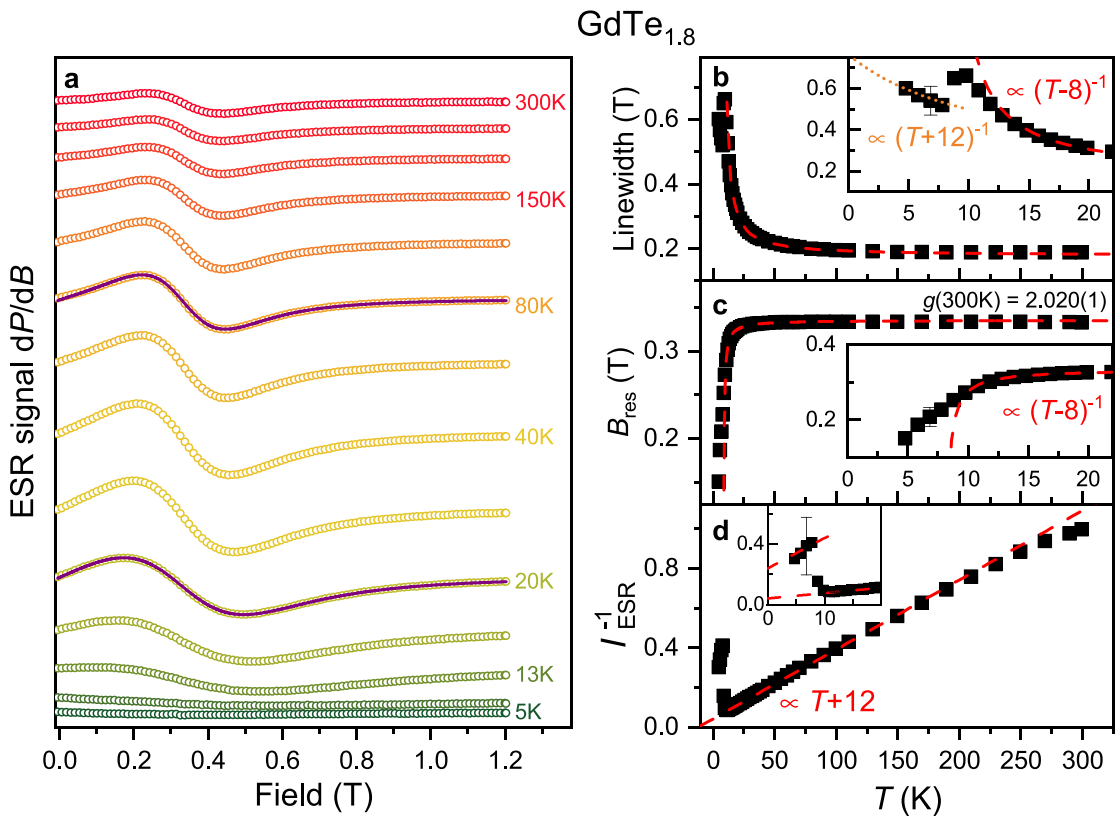

Figure 5. (a) ESR spectra at selected temperatures with solid lines indicating Lorentzian line shapes and temperature dependence of main ESR line parameters (b) linewidth, (c) resonance field and (d) reciprocal ESR intensity, with Curie–Weiss behavior indicated by the dashed and dotted lines, as described in the main text.

in other magnetically ordering rare-earth intermetallics as well [26, 27]. The same value of $\theta = 8$ K also describes the linewidth divergence, see the dashed line in figure 5(b). A critical exponent of –1 in the broadening indicates Gd-spin fluctuations in a 3D Heisenberg ferromagnet [28]. However, below $T \approx 8$ K, the linewidth instead follows a $\propto (T+12)^{-1}$ K divergence pointing to dominant antiferromagnetic Gd spin correlations that prevail in low-temperature broadening. Given these anomalies in the ESR parameters around 10 K and the peculiarities of $\chi(T)$ and $M(H)$ (see figure 2) the following model of magnetism in $GdTe_{1.8}$ evolves. Within the overall antiferromagnetic behavior, a small fraction (≈17%) of correlated Gd spins locally order ferromagnetically below $T \approx 10$ K where they do not contribute to the ESR intensity. This explains the ferromagnetic Curie–Weiss $\theta = +8$ K appearing in the temperature dependence of the linewidth and resonance field. Moreover clear anomalies in $\chi(T)$ and the hysteresis in $M(H, T = 2\,\mathrm{K})$, figure 2, support the presence of ferromagnetic contributions. The majority part of the Gd spins are predominantly antiferromagnetically correlated as indicated by a negative Curie–Weiss $\theta = -12$ K of I_{ESR} and linewidth. In a way this situation is comparable to $EuMn_2P_2$ where in the Eu-ESR signal an anomaly occurred at $T = 47$ K, pointing to weak Mn-based magnetic order [27].

In order to relate the mentioned specific magnetic properties of $GdTe_{1.8}$ to its crystal structure it is rewarding to consider previously reported results for $GdTe_2$ [17], $GdTe_3$ [15, 18, 19, 29] and $GdTe_{1.875\pm\delta}$ [13]. All of these compounds contain puckered GdTe slabs separated by one or two planar Te layers. Their magnetization data all display AFM order features below very similar Néel temperatures of $\leqslant 11$ K while their specific heat curves indicate multiple transition close to T_N.

To the best of our knowledge, there is no experimentally determined or verified structural model of a magnetically ordered structure of $RETe_{2\pm\delta}$ compound which could serve as a basis to explain the observed features which we attribute to the presence of AFM and FM couplings on the atomic scale. For $GdTe_3$ which contains the same GdTe slabs, a fairly simple AFM model with the moments aligned in plane, i.e. perpendicular to the stacking direction was proposed [29]. This situation cannot be transferred to $GdTe_{1.8}$ for symmetry reasons as the Wyckoff site 2*c* (on which Gd1 and Gd4 are located; atom labeling according to [14], ICSD collection code 130 089) does either only allow contributions of the magnetic moment along [001] (in the magnetic space groups P4/n and P4/n') or no contribution at all (in P4'/n and P4'/n') [30]. The Wyckoff site 8*g* (Gd2, Gd3) does not impose any restrictions on the spin

alignment. Thus, it makes sense to assume a gross spin alignment along [001], maybe with some canting of the Gd2 and Gd3 spins. However, any kind of (collinear) antiferromagnetic order in one plane of Gd atoms would necessarily imply both, FM and AFM interactions with the next Gd plane of the GdTe slab, see figure S2 in the Supplementary materials, as the two Gd square planes are shifted against each other so that the Gd atoms of the first plane are located above the voids of the second and vice versa. In contrast to $GdTe_3$, a coupling between two Gd planes of adjacent slabs by superexchange via the atoms of the planar Te layers is likely in $GdTe_{1.8}$ since the '*in-slab*' (3.12 Å – 3.26 Å) and '*out-of-slab*' Gd–Te distances (3.08 Å – 3.39 Å) are very similar in this structure. Most Gd–Te–Gd bond angles for the intra slab connections are around 80±4° and 122±4° whereas the histogram for the '*out-of-slab*' angles shows maxima at 85±4° and 104±4°. Due this diversity of coordination and connectivities, the application of Goodenough–Kanamori–Anderson rules to predict a certain type of magnetic interaction is difficult. However, Ruderman–Kittel–Kasuya–Yosida type interaction between the Gd atoms of different slabs, as discussed for $GdTe_3$ [29], can be excluded since $GdTe_{1.8}$ is a semiconductor.

4. Conclusions

Polycrystalline $GdTe_{1.8}$ was synthesized in order to investigate its local magnetic properties. From C_p data, the magnetic entropy was estimated, and is less than the theoretical value at zero field, likely due to residual crystal-field effects and magnetic interactions. Large negative magnetoresistance at low temperatures is observed, where at $T = 2$ K ρ drops an order of magnitude at a magnetic field of 9 T. ESR measurements show clear anomalies in both the linewidth and the intensity at temperatures near 10 K, also observed in magnetization and in our data of C_p, corroborating ferro- and antiferromagnetically correlated nature of this material which can be rationalized by structural and symmetry arguments. However, an explanation on the atomic scale is still pending and should facilitate further research and exploration on this and similar chalcogenides.

Acknowledgments

We thank Michael Baenitz for valuable discussions. The National High Magnetic Field Laboratory is supported by the National Science Foundation through NSF/DMR-1644779, NSF/DMR-2128556, and the State of Florida.

Data availability statement

All data that support the findings of this study are included within the article (and any supplementary files).

Suppl. material contains two Figures available at: https://doi.org/10.1088/1361-648X/ae8aa1/data1.

Author contributions

Jörg Sichelschmidt 0000-0001-8282-3139
Investigation (equal), Writing – original draft (equal)

Ellen Häußler 0000-0001-5620-836X
Investigation (supporting)

Jorge Galeano-Cabral
Investigation (supporting)

Kaya Wei
Investigation (supporting)

Thomas Doert 0000-0001-7523-9313
Project administration (equal), Writing – original draft (equal)

George S Nolas 0000-0001-8741-1678
Project administration (equal), Writing – review & editing (equal)

References

[1] Lei S *et al* 2020 *Sci. Adv.* **6** eaay6407
[2] Jiang B, Wang W, Liu S, Wang Y, Wang C, Chen Y, Xie L, Huang M and He J 2022 *Science* **377** 208–13
[3] Raoux S, Wełnic W and Ielmini D 2010 *Chem. Rev.* **110** 240–67
[4] Klingner C *et al* 2011 *Phys. Rev. B* **83** 144405
[5] Rauch D *et al* 2015 *Phys. Rev. B* **91** 174404
[6] Senapati K, Fix T, Vickers M E, Blamire M G and Barber Z H 2011 *Phys. Rev. B* **83** 014403
[7] Chen X *et al* 2024 *Phys. Rev. B* **109** 224428
[8] Kitagawa J, Yakabe G, Nakayama A, Nishizaki T and Tsubota M 2020 *J. Solid State Chem.* **284** 121188
[9] Pérez N, Casanova F, Bartolomé F, García L M, Labarta A and Batlle X 2011 *Phys. Rev. B* **83** 184411
[10] Opletal P, Fikáček J, Duverger-Nédellec E, Thamizhavel A, Hossain Z, Tarasenko R, Tkáč V, Legut D, Shen B, Gegenwart P and Custers J 2026 (arXiv:2605.31118)
[11] Doert T and Müller C J 2016 *Reference Module in Chemistry, Molecular Sciences and Chemical Engineering* (Elsevier)
[12] Doert T, Poddig H and Finzel K 2023 *Z. Anorg. All. Chem.* **649** e202300118
[13] Poddig H, Gebauer P, Finzel K, Stöwe K and Doert T 2021 *Inorg. Chem.* **60** 11231–41
[14] Poddig H, Donath T, Gebauer P, Finzel K, Kohout M, Wu Y, Schmidt P and Doert T 2018 *Z. Anorg. All. Chem.* **644** 1886
[15] Iyeiri Y, Okumura T, Michioka C and Suzuki K 2003 *Phys. Rev. B* **67** 144417
[16] Karki Chhetri S *et al* 2025 *Phys. Rev. B* **111** 014431
[17] Min B, Cho J, Lee H, Han C, Kim D and Kwon Y 2000 *Physica B* **281-282** 118–9
[18] Ru N, Chu J H and Fisher I R 2008 *Phys. Rev. B* **78** 012410
[19] Guo Q, Bao D, Zhao L and Ebisu S 2021 *Physica B* **617** 413153
[20] García D J, Sereni J G and Aligia A A 2026 *Phys. Rev. B* **113** 054410
[21] Zeleňák V, Almáši M, Zeleňáková A, Hrubovč ák P, Tarasenko R, Bourelly S and Llewellyn P 2019 *Sci. Rep.* **9** 15572
[22] Bouvier M, Lethuillier P and Schmitt D 1991 *Phys. Rev. B* **43** 13137–44
[23] Pecharsky V K and Gschneidner, Jr. J K A 1997 *Phys. Rev. Lett.* **78** 4494–7
[24] Law J Y, Moreno-Ramírez L M, Díaz-García A and Franco V 2023 *J. Appl. Phys.* **133** 040903
[25] Glasbrenner J K, Belashchenko K D, Kudrnovský J, Drchal V, Khmelevskyi S and Turek I 2012 *Phys. Rev. B* **85** 214405
[26] Taylor R H 1975 *Adv. Phys.* **24** 681
[27] Krebber S *et al* 2025 *Phys. Rev. B* **111** 174406
[28] Benner H and Boucher J P 1990 *Spin Dynamics in the Paramagnetic Regime: Nmr and epr in two-Dimensional Magnets* (*Physics and Chemistry of Materials With Low-Dimensional Structures)* vol 9 L J De Jongh ((Dordrecht: Kluwer) review Magnetic Properties of Layered Transition Metal Compounds) pp 323–78
[29] Liu J S *et al* 2020 *Phys. Rev. Mater.* **4** 114005
[30] Litvin D B 2013 *Magnetic Group tables: 1-, 2- and 3-Dimensional Magnetic Subperiodic Groups and Magnetic Space Groups* 1st edn (International Union of Crystallography)